

# A study of the influence of synthesis parameters on the physicochemical properties of iron pigments produced from waste iron sulfate

Kamila Splinter<sup>ID</sup>, Zofia Lendzion-Bielun<sup>\*</sup><sup>ID</sup>

West Pomeranian University of Technology in Szczecin, Faculty of Chemical Technology and Engineering,  
Department of Inorganic Chemical Technology and Environment Engineering, Piastów 42, 71-065 Szczecin, Poland

## \* Corresponding author:

e-mail:

[Zofia.lendzion-bielun@zut.edu.pl](mailto:Zofia.lendzion-bielun@zut.edu.pl)

Presented at 24th Polish Conference of Chemical and Process Engineering, 13–16 June 2023, Szczecin, Poland.

## Article info:

Received: 27 April 2023

Revised: 12 June 2023

Accepted: 29 June 2023

## Abstract

The work presents a two-step method of iron red synthesis based on waste iron(II) sulfate. The synthesis was carried out using purified waste iron sulfate from titanium dioxide production. The study investigated the influence of factors such as temperature, pressure, concentration of solutions and synthesis time on the physicochemical properties of pigments. Obtained pigments were tested with instrumental analytical methods, e.g. X-ray Diffraction or BET surface area analysis. The pigments were analyzed for color, particle size as well as for oil number. The results of the research showed a change in the physicochemical properties of the obtained pigments depending on the conditions of synthesis. It was shown that increasing the synthesis time in most cases increased the degree of crystallization of hematite in the pigments. High specific surface area, low agglomeration of pigments or low oil absorption were directly related to the crystallinity of the pigments obtained. Laboratory pigments have been found to be different from commercial pigments. The difference in properties speaks in favor of synthesized materials.

## Keywords

hematite, iron red, iron pigment, pigment

## 1. INTRODUCTION

Iron pigments are probably the most well-known group of materials. They are non-toxic which makes them phenomenal to be used in a variety of fields from coloring building materials (Amiri et al., 2022; Fortuño-Morte et al., 2020; Gramm et al., 2020; Pfaff, 2021), food and medicaments (Pfaff, 2022; Sander, 2020; Sarkodie et al., 2019) to cosmetic pigments (Pagès et al., 2020; Pérez-Arantegui, 2021; Pfaff, 2021). Their high chemical resistance as well as ease of synthesis and low cost production allow for high-scale production (Lu et al., 2020; Salgado Lopes et al., 2019; Siqueira-Silva et al., 2019). In the iron pigment industry, the most common processes are the precipitation and the Penniman Zoph process (Krześlak et al., 2005). Both of these processes can produce pigments with a wide range of colors, characteristic of iron oxides and oxyhydroxides. In this way, with minor process modifications, it is possible to synthesize yellow, orange, red, and black pigments.

Scientists also frequently address the topic of iron pigments and synthesis parameters affecting the physicochemical properties of this materials. The most well-known parameter affecting the properties of hematite is temperature. The authors of the publication (Touazi et al., 2020) studied the effect of calcination temperature on the properties of iron pigments. Hematite was obtained by calcining FeOOH at

temperatures of 200 °C, 500 °C and 900 °C. The oxides obtained at 200 and 500 °C were characterized by a “wire-like” structure, while at 900 °C highly crystallized hematite was obtained. The material calcined at 900 °C was also characterized by much lower porosity, than the other materials. All of the materials showed very high particle agglomeration with major particle size in the range of 10–80 μm.

Similar conclusions about the effect of temperature on the properties of hematite were reached by the authors of several other publications (Mariani et al., 2017; Sreeram et al., 2006). In each of them, materials calcined at low temperatures (200–300 °C) showed a highly amorphous structure with a small proportion of hematite and also higher porosity than those reported in the literature for hematite. At materials calcined at temperatures above 400 °C, a significant reduction in porosity was observed as well as a reduction in the amount of amorphous phase. At the same time, the particles of pigments at high temperature were characterized by small size (about 200–300 nm).

The effect of pressure has been demonstrated for reactions with hydro- and solvo-thermal methods. The hydrothermal method is based on a reaction between suitable reactants in an aqueous environment. The reaction takes place under conditions of increased temperature and pressure – for this reason it is often carried out in autoclaves or microwave reactors. Reagents can be dissolved in the medium or be in suspension



form. The materials synthesized can be obtained by hydrolysis or recrystallization of the reactants under hydrothermal conditions. Advantages of the hydrothermal method include the ability to control the growth of crystallites, which eliminates the phenomenon of agglomeration and formation of heterogeneous crystals. By monitoring the reaction parameters (time and temperature), pure and homogeneous products (Cornell et al., 1987; Diamandescu et al., 1996).

Majority of works addressed the hydrothermal method as its application in the synthesis of hematite. It was shown that the transition temperature of goethite ( $\alpha$ -FeO(OH)) into hematite ( $\alpha$ -Fe<sub>2</sub>O<sub>3</sub>) is about 200 °C (Barb et al., 1990; Benhammada et al., 2020). It was also proven that the conditions of the process, such as pH, temperature, type of precipitating agent, clearly affected the morphology and physicochemical properties of the particles (Benhammada et al., 2020; Tadic et al., 2019).

The use of a microwave reactor, which has the ability to carry out a reaction under increased pressure, allows similar results to be obtained at much lower than standard temperatures. That is, if goethite under normal conditions transforms into hematite at a temperature of about 500 °C, then using a microwave reactor and carrying out this transformation under high pressure will allow us to lower the temperature of the transformation to about 260 °C (Benhammada et al., 2020; Diamandescu et al., 1999). At the same time, the lower fusion temperature favors the formation of particles of smaller size.

Undoubtedly, the use of microwave reactor synthesis, allows very rapid and uniform heating of a given medium, increasing the reaction rate and shortening its time (Splinter and Lendzion-Bieluń, 2021; Splinter et al., 2023). In addition, the materials obtained with this method have high quality (low agglomeration, higher chemical resistance) compared to compounds obtained with other methods (Nambodiri and Verma, 2001). The authors of the publication (Bensebaa et al., 2004), however, point out the instability of microwave systems in terms of temperature. During the process, the temperature varies depending on the microwave power – thus, particles can be in different sizes.

Due to many variables affecting the synthesis of hematite, it is difficult to choose one suitable synthesis method. However, learning about the influence of certain parameters makes it possible to find the optimal reaction conditions, depending on what type of pigments are wanted to obtain.

However, our preliminary research showed that it is possible to reduce temperature of iron(III) hydroxide-goethite-hematite phase transition to temperature lower than 200 °C and obtain pigments with high-crystallized hematite phase. In addition, iron red based on long-deposited waste iron(II) sulfate has different physicochemical properties in comparison to commercial pigments synthesized from pure reagents (Splinter et al., 2023). Based on preliminary research, this

study showed the influence of synthesis parameters for physicochemical properties of iron pigments. Parameters chosen in a microwave-based reaction are: pressure, time of reaction and iron salt solutions concentration.

## 2. EXPERIMENTAL

### 2.1. Materials

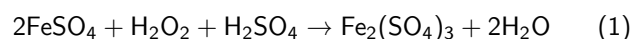
Waste FeSO<sub>4</sub> from Grupa Azoty Zakłady Chemiczne Police was used. Salt was long-deposited 1972–2012 and contains many impurities. The main contaminants are titanium, manganese and light metal ions. Waste iron sulfate is also an oxidized salt and contains a significant amount of Fe<sup>3+</sup> ions (> 9%). The method described in the publications and patent (Splinter and Lendzion-Bieluń, 2021; Splinter et al., 2021; 2023) was used to purify the salt. The purified salt was the reagent for the synthesis of iron pigments.

Reagent purity substances were also used: 25 wt% ammonia water (Chempur, Poland), and 30 wt% hydrogen peroxide (Chempur, Poland).

### 2.2. Preparation of pigments

The effect of the concentration of starting solutions on the synthesis of iron pigments was investigated. For this purpose, salt solutions with concentrations of 10 and 14 wt% of purified FeSO<sub>4</sub> were prepared. Then two concentrations were chosen based on preliminary research (Splinter, 2021; 2022; Splinter et al., 2023).

First, the assumed amounts of purified FeSO<sub>4</sub> (7.5 g or 10 g) were stirred at room temperature until they formed a transparent light-green solution in aqua (~ 15 ml). For the oxidation, stoichiometric amounts of hydrogen peroxide (30 wt%) were used (1).



Then, to precipitate iron(III) hydroxide, 25 wt% ammonia water was added until pH = 10.25 (2).



Suspension was then transferred into a Teflon container, filled with water to a volume of 70 ml, and placed in the microwave reactor (Ertec Magnum II). As the study focused on the effects of various synthesis factors on the properties of pigments, the reaction time ranged from 1 to 3 hours and the set pressure in ranges of 7–10 or 17–20 bar in a temperature of 170 °C. Due to the use of a microwave reactor, minimum and maximum pressure settings are required. The difference of 3 bar is the minimum difference of pressure to ensure proper operation of the reactor. At the end of the

stage, the obtained suspensions were washed with water and dried at 105 °C for 4 hours.

In order to distinguish between samples, names were introduced according to the example: CZ14% 10B 1h, meaning that the sample was synthesized from a concentration of 14 wt%, for one hour at a pressure in the 7–10 bar range.

### 3. RESULTS AND DISCUSSION

#### 3.1. X-Ray powder diffraction analysis

XRPD patterns were collected with an X-ray diffractometer (Empyrean, Malvern Panalytical, Malvern, United Kingdom) equipped with a Cu-K $\alpha$  radiation source (40 kV, 35 mA). Scans were taken at room temperature in scattering  $2\theta$  range of 10–100° with a step interval of about 0.026°. Phase composition was determined using Panalytical X'Pert HighScore Plus v3.0 software with the ICDD PDF4+ database.

Figure 1 and 2 show diffractograms of pigments synthesized in pressure ranges of 7–10 and 17–20 bar.

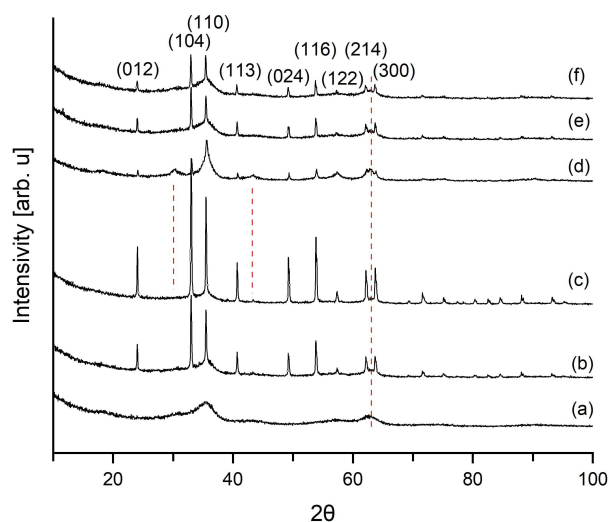


Figure 1. XRPD patterns of laboratory pigment samples synthesized in pressure range of 7–10 bar: (a) CZ 10% 10B 1h, (b) CZ 10% 10B 2h, (c) CZ 10% 10B 3h, (d) CZ 14% 10B 1h, (e) CZ 14% 10B 2h, (f) CZ 14% 10B 3h. Red lines indicated goethite remnants.

It can be seen that the samples consist of hematite (ICDD No.:00-024-0072). Samples synthesized in pressure range of 7–10 bar contain, in addition to partially crystallized compounds, a significant amount of the amorphous phase. The broad bases of the reflection (110) suggest that hematite was formed by dehydration of goethite (Wolska and Schwertmann, 1989; Wolska, 1988). Red lines indicate places where goethite remnants can be seen in the diffraction pattern – the most characteristic group of three peaks in a range of

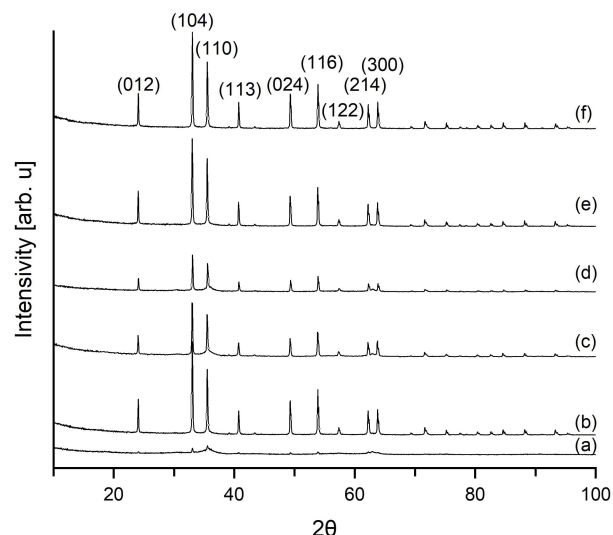


Figure 2. XRPD patterns of laboratory pigment samples synthesized in pressure range of 17–20 bars: (a) CZ 10% 20B 1h, (b) CZ 10% 20B 2h, (c) CZ 10% 20B 3h, (d) CZ 14% 20B 1h, (e) CZ 14% 20B 2h, (f) CZ 14% 20B 3h.

62–64  $2\theta$  are shown (ICDD No.: 01-073-8431). Samples synthesized at 17–20 bar show high crystallinity. The size of hematite crystallites exceeds 100 nm.

At lower concentrations and using low pressure, increasing the synthesis time increases the crystallinity of the materials (CZ 10% 10B 1h, CZ 10% 10B 2h and CZ 10% 10B 3h). In order for the same increase in crystallinity to occur at higher concentrations, the synthesis pressure (CZ 14% 20B 1h, CZ 14% 20B 2h and CZ 14% 20B 3h) must be raised in addition to extending the time. Moreover, increasing the synthesis time with high pressure and low concentrations results in a decrease in the crystallinity of the material (CZ 10% 20B 3h). The mechanism for such a phenomenon may be related to hematite crystallization. The crystal grows at a certain concentration, which changes over time (Arinchtein et al., 2020; Su et al., 2011). Increasing the time of synthesis we exceed the point of crystal growth, causing breakdown of the already obtained structure (Fouad et al., 2019; Wang et al., 2022).

#### 3.2. Specific surface area

The specific surface area of pigments was determined with the Brunauer-Emmett-Teller (BET) method using the Quadrasorb Evo Quantachrome Instruments nitrogen adsorption apparatus. A sample was degassed at 100 °C under a high vacuum for 16 hours. Figure 3 shows nitrogen adsorption and desorption isotherms for synthesized materials.

Obtained pigments have an isotherm shape corresponding to type V in according to the IUPAC classification (Rouquerol et al., 1994; Sing et al., 1985). It is characteristic of mesoporous

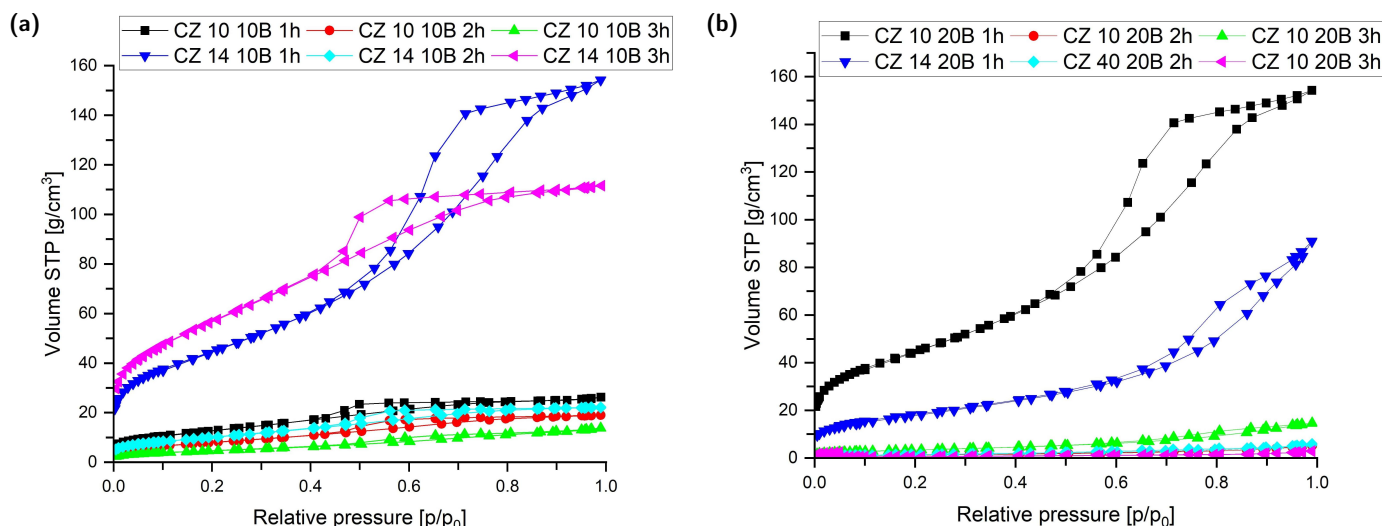


Figure 3. Results obtained from BET analysis. Nitrogen adsorption isotherms of pigments synthesized in pressure range of: (a) 7–10 bar, (b) 17–20 bar.

materials. The hysteresis shape corresponds to E type, i.e. spherically elongated or bottle-shaped pores with open ends. The shape of the adsorption isotherms for pigments synthesized in pressure range of 17–20 also correspond to isotherms for mesoporous materials, but with a much lower adsorption capacity.

Synthesized pigments have up to 25 times greater specific surface area than commercial pigments (values up to 10 m<sup>2</sup>/g) (Splinter et al., 2023). Specific surface area value mostly decreases with increasing crystallinity of hematite in materials which can be seen in Figure 4. In the literature (Arbain et al., 2011; Dehbi et al., 2020; Jozwiak et al., 2007; Sander, 2020) goethite-hematite phase transition temperature is 450 °C. Hematite obtained at this temperature has a specific surface area in the range of 25–40 m<sup>2</sup>/g. By contrast, pigment industry usually uses calcination method to obtain pigment structure. It takes place at  $a > 700$  °C for 10 to 20 hours (Kamel et al., 1972; Krześlak et al., 2005;

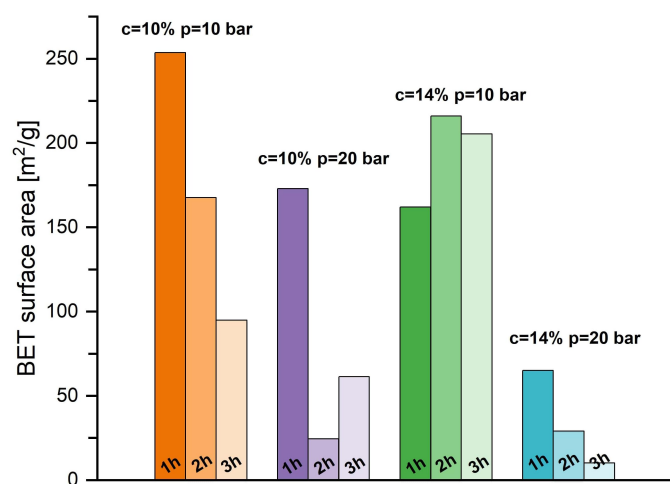


Figure 4. BET surface area of laboratory pigments.

Sarkodie et al., 2019). In this study, the phase transition during synthesis takes place at a temperature of about 160 °C, which further promotes a higher specific surface area.

In the case of synthesized pigments in pressure range of 7–10, it cannot be said that the higher the amorphous phase content in the samples, the higher the specific surface area of the material. Samples synthesized in pressure range of 17–20 bars (CZ 10% 20B 2h, CZ 10% 20B 3h, CZ 14% 20B 1h, CZ 14% 20B 2h, CZ 14% 20B 3h), containing well-crystallized hematite, have the value of the specific surface area close to the value in the literature (Arbain et al., 2011; Khanam et al., 2023).

### 3.3. Particle size distribution

Dynamic light scattering measurements (DLS) were carried out on the Horiba LA 950 Laser Diffraction Particle Size Analyzer. A sample was dispersed in 50 ml of 0.1% sodium pyrophosphate solution. Then, the solution was sonicated in an ultrasonic cleaner for 2 minutes. The prepared dispersion was loaded into the analyzer. In the measurements, a reflectance coefficient of 2.90 was used, and sonication was turned on.

Figures 5 and 6 show particle size distribution for obtained pigments. At a pressure of 7–10 bar, the proportion of particles with a size of 0.1–3 μm does not exceed 40%, while at a pressure of 17–20 bar, the proportion of particles in this range is higher and is about 90% for most samples. Increasing the pressure results in samples with a narrower size distribution.

The CZ 10% 10B 2h, CZ 10% 10B 3h, CZ 10% 20B 1h, CZ 10% 20B 2h and CZ 14% 20B 1h samples have the highest proportion of particles in the range of 100–500 nm. Some samples tend to show particle agglomeration. This is evidenced by either two maxima of particle size distribution or

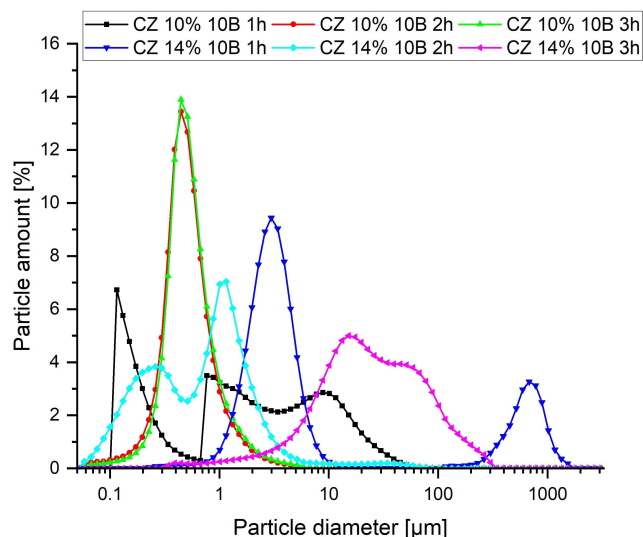


Figure 5. Pigment size distribution analysis by dynamic light scattering of pigments synthesized at 7–10 bar.

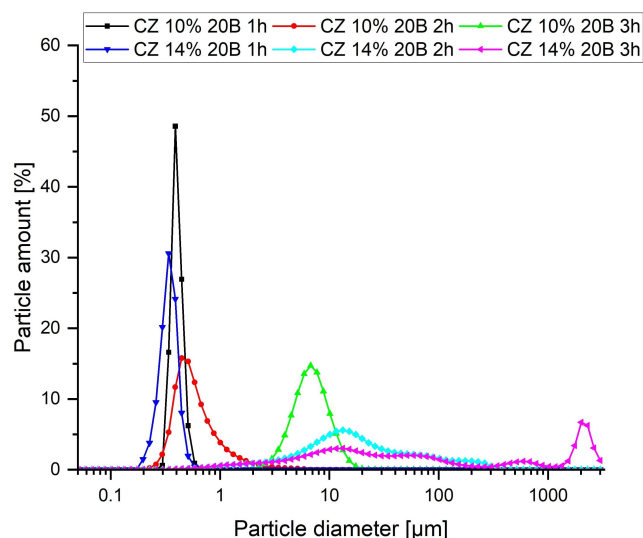


Figure 6. Pigment size distribution analysis by dynamic light scattering of pigments synthesized at 17–20 bar.

one maximum shifted toward larger values of particle diameter e.g. CZ 10% 10B 1h, CZ 14% 10B 1h or CZ 14% 20B 3h.

### 3.4. Surface morphology

The surface morphology of samples was observed with an emission scanning electron microscope VEGA 3 (TESCAN, Brno, Czech Republic). A sample was dispersed in isopropyl alcohol, and 2 μl were placed on silicon wafers and evaporated.

SEM images are shown in Figures 7 and 8. Most of the synthesized materials have agglomerates < 1 μm. The lowest aggregates are shown in CZ 10% 10B 3h, CZ 10% 20B 2h and CZ 10% 20B 3h samples. There are many agglomerates mostly under 500 nm in size.

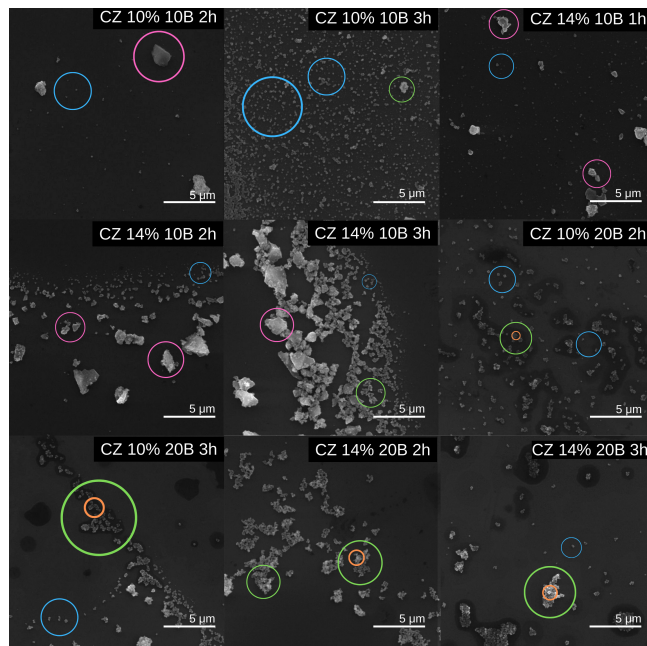


Figure 7. SEM images of iron pigments (SEM HV: 30 kV; SEM MAG: 30 kx).

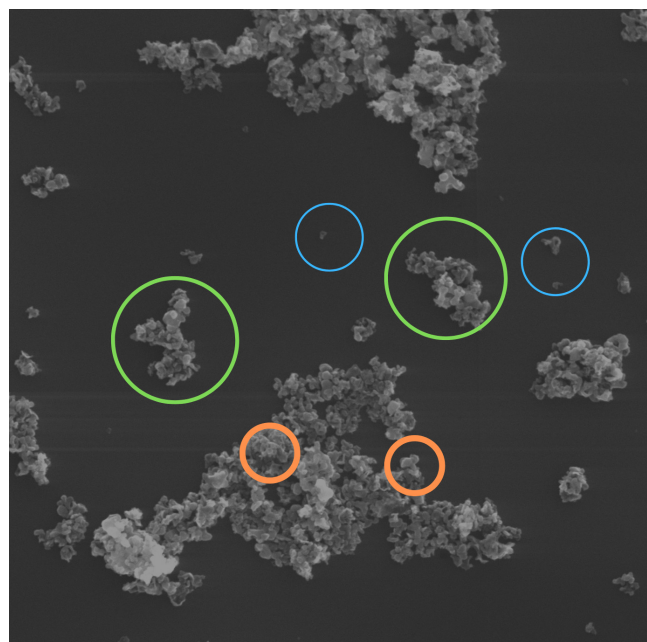


Figure 8. SEM images of commercial iron pigment (SEM HV: 30 kV; SEM MAG: 30 kx).

Blue particles are single particles up to 500 nm in size. Agglomerates of particles > 500 nm with single particles highlighted are green. Orange granules are individual particles forming agglomerates with a size of 100–600 nm. Pink particles are aggregates of particles < 2 μm with indistinguishable single particles.

Obtained pigments show agglomeration. In comparison with commercial pigment, agglomeration of laboratory materials

is decreased. It can be connected to high specific surface area of the materials.

CZ 14% 20B 3h sample has somewhat interesting structure. Most of obtained pigments are spherical-like particles while CZ 14% 20B 3h sample is cubical. Some cube structure is also visible in CZ 10% 20B 2h, CZ 10% 20B 3h and CZ 14% 20B 2h samples. It can be connected with high crystallinity of the materials (Su et al., 2011; Wang et al., 2022).

### 3.5. Oil absorption

Oil absorption was determined according to the PN-EN ISO 787-5:1999 standard.

Commercial pigments should have an oil absorption of a maximum of 35 g/100 g based on the product technical sheets. This value was considered a reference value. Most obtained pigments were characterized by a lower or equal oil absorption value (Fig. 9). Oil absorption mostly decreases with higher pressure and longer sample synthesis time, which is connected with crystallinity of the materials.

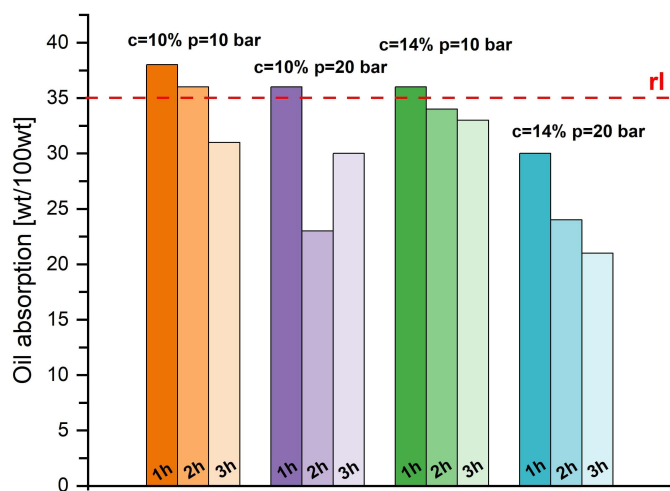


Figure 9. Oil absorption for laboratory and commercial pigments. rl – reference level.

### 3.6. Color analysis

Color analysis was conducted with hand spectrophotometer (Konica Minolta, CM-700d, Japan). Spectrometer was calibrated on white standard and three measurements for each sample were done. The CIELAB scale was used to measure pigment color. This scale is based on the theory of opposing colors, assuming that receptors in the human eye perceive colors as pairs of opposites. Designed in this way, the scale allows a given color to be placed in three-dimensional space, using three values –  $L$ ,  $a$  and  $b$  – to describe each color (Fig. 10).

The value of  $L$  allows to determine how light or how dark the sample is, the value of  $a$  determines the redness or greenness

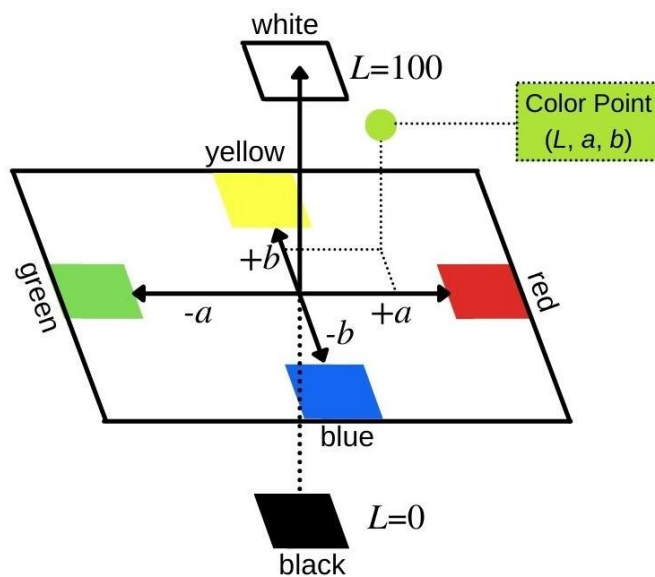


Figure 10. Graphical representation of the CIELAB color scale in a three-dimensional system (Stockman and Gevers, 2000).

of the sample while the value of  $b$  indicates whether the color is more warm, yellow, or cold, blue (Durmus, 2020; Mielicki, 1997; Stockman and Gevers, 2000).

To determine the color difference between the samples, the formula was used:

$$\Delta E = \sqrt{(\Delta L)^2 + (\Delta a)^2 + (\Delta b)^2} \quad (3)$$

It is assumed that a standard observer notices the color difference as follows:

- $0 < \Delta E < 1$  – does not notice the difference,
- $1 < \Delta E < 2$  – only an experienced observer notices the difference,
- $2 < \Delta E < 3.5$  – an inexperienced observer also notices the difference,
- $3.5 < \Delta E < 5$  – notices a clear color difference,
- $5 < \Delta E$  – the observer gets the impression of two different colors (Mielicki, 1997; Stockman and Gevers, 2000).

Table 1 shows average  $L$ ,  $a$ ,  $b$  and  $\Delta L$  values and conversion CIELAB scale to HEX scale with colors of obtained pigments.

All of the samples are  $+a$  and  $+b$  space, which means that colors are warm and reddish. Luminance of samples is on  $L \sim 25$  (referenced to the target white standard  $L = 99.18$ ,  $a = -0.10$  and  $b = -0.13$ ), which means that they are darker than the white standard, but still lighter than pure black ( $L = 0$ ). The darker color of the pigments is related to the small particle size ( $< 500$  nm) as can be seen in SEM images. Luminance of samples is on the average level for dark red pigments (Ding et al., 2019; Gong et al., 2023; Splinter and Lendzion-Bieluń, 2021).

Table 1. Summary of  $L$ ,  $a$ ,  $b$  and  $\Delta E$  values for samples. The color codes are given in hexadecimal (HEX) (Color converter).

Sample	$L$	$a$	$b$	$\Delta E$	Color codes (HEX)	Color
CZ 10% 10B 1h	28.09	12.00	10.83	72.94	#583B32	
CZ 10% 10B 2h	25.13	11.80	8.84	75.53	#50352F	
CZ 10% 10B 3h	25.08	15.46	10.02	76.40	#54322D	
CZ 10% 20B 1h	21.48	6.34	5.00	78.19	#3F302C	
CZ 10% 20B 2h	31.35	20.96	12.29	72.10	#6C3C38	
CZ 10% 20B 3h	25.72	15.57	10.62	75.88	#56332E	
CZ 14% 10B 1h	22.24	7.29	6.12	77.55	#42312C	
CZ 14% 10B 2h	25.29	11.21	8.56	72.25	#4F3530	
CZ 14% 10B 3h	25.98	12.03	8.78	74.73	#523631	
CZ 14% 20B 1h	28.75	20.24	10.14	74.03	#633735	
CZ 14% 20B 2h	29.28	19.11	11.17	73.37	#643935	
CZ 14% 20B 3h	29.53	21.18	10.79	73.65	#673836	

## 4. CONCLUSIONS

This study showed the influence of synthesis parameters on physicochemical properties of iron pigments. The main finding is that a decrease of temperature to 170 °C with a slight increase of pressure (up to 20 bars) allows to produce iron reds with high fine-crystallized hematite content. The optimal concentration of salt solution is 14 wt%, because regardless of the synthesis time, the pigments obtained in the 17–20 bar range have high crystallinity. Time matters in the case of low pressure in the 7–10 bar range. A longer synthesis at a lower concentration allows high crystallization of hematite.

The resulting materials have a high specific surface area, higher than commercially obtained pigments. Increasing the pressure and lengthening the synthesis time reduces the specific surface area. The increase of pressure also increases the proportion of low-size particles, resulting in a darker color of pigments. At the same time, increasing the synthesis time causes the material particles to show higher agglomeration.

The most similar values of oil absorption to commercial pigments are those synthesized at 14 wt% concentration regardless of the applied pressure and synthesis time. It is related to the high crystallization of hematite in the samples. The hematite crystallites in the samples have a high specific surface area that increases the oil absorption capability. This indicates that concentration is an important parameter to consider when synthesizing oil absorbing pigments. The resulting pigments are characterized by their dark color.

The results obtained allow to assume that these pigments can be used in the paint or building material industry. The

low oil absorption or high specific surface area of the pigments can be an advantage for coloring building materials. The dark shade of the pigments can be a problem in the production of paints. However, there are ways to lighten the color with the help of nanofillers, e.g. TiO<sub>2</sub> or chalk. However, determining the application of the resulting pigments still requires research.

To conclude, stable synthesis conditions in a microwave reactor make it possible to obtain iron red. The pressure, the time of synthesis and also the concentration of reactants have a significant effect on the properties of the materials obtained. However, by selecting the parameters in an appropriate way, it is possible to control the particle size or specific surface area of the material.

## ACKNOWLEDGEMENTS

Part of the research was carried out under the “Najlepsi z Najlepszych 4.0” grant (MEiN/2021/182/DIR/NN4) under the Ministry of Education and Science Republic of Poland and Knowledge Education Development Operational Program Co-financed by the European Social Fund.

## REFERENCES

- Amiri M., Sanjari M., Porhonor F., 2022. Microstructural evaluation of the cement stabilization of hematite-rich red soil. *Case Stud. Constr. Mater.*, 16, e00935. DOI: [10.1016/J.CSCM.2022.E00935](https://doi.org/10.1016/J.CSCM.2022.E00935).
- Arbain R., Othman M., Palaniandy S., 2011. Preparation of iron oxide nanoparticles by mechanical milling. *Miner. Eng.*, 24, 1–9. DOI: [10.1016/J.MINENG.2010.08.025](https://doi.org/10.1016/J.MINENG.2010.08.025).
- Arinchtein A., Schmack R., Kraffert K., Radnik J., Dietrich P., Sachse R., Kraehnert R., 2020. Role of water in phase transformations and crystallization of ferrihydrite and hematite. *ACS Appl. Mater. Interfaces*, 12, 38714–38722. DOI: [10.1021/acami.0c05253](https://doi.org/10.1021/acami.0c05253).
- Barb D., Diamandescu L., Mihăilă-Tărăbăsanu D., Rusi A., Morariu M., 1990. Mössbauer spectroscopy study on the hydrothermal transformation  $\alpha$ -FeOOH  $\rightarrow$   $\alpha$ -Fe<sub>2</sub>O<sub>3</sub>. *Hyperfine Interact.*, 53, 285–289. DOI: [10.1007/BF02101054](https://doi.org/10.1007/BF02101054).
- Benhammada A., Trache D., Kesraoui M., Chelouche S., 2020. Hydrothermal synthesis of hematite nanoparticles decorated on carbon mesospheres and their synergetic action on the thermal decomposition of nitrocellulose. *Nanomaterials*, 10, 968. DOI: [10.3390/NANO10050968](https://doi.org/10.3390/NANO10050968).
- Bensebaa F., Zavaliche F., Ecuyer P.L., Cochrane R.W., Veres T., 2004. Microwave synthesis and characterization of Co – ferrite nanoparticles. *J. Colloid Interface Sci.*, 277, 104–110. DOI: [10.1016/j.jcis.2004.04.016](https://doi.org/10.1016/j.jcis.2004.04.016).
- Color converter. Available at: <https://www.nixsensor.com/Free-Color-Converter/>.
- Cornell R.M., Givanali R., Schindler P.W., 1987. Effect of silicate species on the transformation of ferrihydrite into goethite and

- hematite in alkaline media. *Clays Clay Miner.*, 35, 21–28. DOI: [10.1346/CCMN.1987.0350103](https://doi.org/10.1346/CCMN.1987.0350103).
- Dehbi A., Dehmani Y., Omari H., Lammini A., Elazhari K., Abdallaoui A., 2020. Hematite iron oxide nanoparticles ( $\alpha$ -Fe<sub>2</sub>O<sub>3</sub>): Synthesis and modelling adsorption of malachite green. *J. Environ. Chem. Eng.*, 8, 103394. DOI: [10.1016/J.JECE.2019.103394](https://doi.org/10.1016/J.JECE.2019.103394).
- Diamandescu L., Mihaila-Tarabaşanu D., Popescu-Pogrion N., 1996. Hydrothermal transformation of  $\alpha$ -FeOOH into  $\alpha$ -Fe<sub>2</sub>O<sub>3</sub> in the presence of silicon oxide. *Mater. Lett.*, 27, 253–257. DOI: [10.1016/0167-577X\(95\)00295-2](https://doi.org/10.1016/0167-577X(95)00295-2).
- Diamandescu, L., Mihaila-Tarabaşanu D., Popescu-Pogrion N., Totovina A., Bibicu I., 1999. Hydrothermal synthesis and characterization of some polycrystalline  $\alpha$ -iron oxides. *Ceram. Int.*, 25, 689–692. DOI: [10.1016/S0272-8842\(99\)00002-4](https://doi.org/10.1016/S0272-8842(99)00002-4).
- Ding X., Yu M., Wang Z., Zhang B., Li L., Li J., 2019. A promising clean way to textile colouration: cotton fabric covalently-bonded with carbon black, cobalt blue, cobalt green, and iron oxide red nanoparticles. *Green Chem.*, 21, 6611–6621. DOI: [10.1039/C9GC02084E](https://doi.org/10.1039/C9GC02084E).
- Durmus D., 2020. CIELAB color space boundaries under theoretical spectra and 99 test color samples. *Color Res. Appl.*, 45, 796–802. DOI: [10.1002/COL.22521](https://doi.org/10.1002/COL.22521).
- Fortuño-Morte M., Beltrán-Mir H., Cordoncillo E., 2020. Study of the role of praseodymium and iron in an environment-friendly reddish orange pigment based on Fe doped Pr<sub>2</sub>Zr<sub>2</sub>O<sub>7</sub>: A multifunctional material. *J. Alloys Compd.*, 845, 155841. DOI: [10.1016/J.JALLCOM.2020.155841](https://doi.org/10.1016/J.JALLCOM.2020.155841).
- Fouad D.E., Zhang C., El-Didamony H., Yingnan L., Mekuria T.D., Shah A.H., 2019. Improved size, morphology and crystallinity of hematite ( $\alpha$ -Fe<sub>2</sub>O<sub>3</sub>) nanoparticles synthesized via the precipitation route using ferric sulfate precursor. *Results Phys.*, 12, 1253–1261. DOI: [10.1016/J.RINP.2019.01.005](https://doi.org/10.1016/J.RINP.2019.01.005).
- Gong L., Hua X., Yao B., Liang J., Tian G., 2023. Novel red composite pigment with high thermostability from iron ore tailings: Synthesis and coloring mechanism. *Ceram. Int.*, 49, 5066–5076. DOI: [10.1016/J.CERAMINT.2022.10.021](https://doi.org/10.1016/J.CERAMINT.2022.10.021).
- Gramm G., Fuhrmann G., Zimmerhofer F., Wieser M., Hupertz H., 2020. Development of high NIR-reflective red Li<sub>2</sub>MnO<sub>3</sub> pigments. *Z. Anorg. Allg. Chem.*, 646, 1722–1729. DOI: [10.1002/ZAAC.202000274](https://doi.org/10.1002/ZAAC.202000274).
- Jozwiak W.K., Kaczmarek E., Maniecki T.P., Ignaczak W., Maniukiewicz W., 2007. Reduction behavior of iron oxides in hydrogen and carbon monoxide atmospheres. *Appl. Catal., A*, 326, 17–27. DOI: [10.1016/J.APCATA.2007.03.021](https://doi.org/10.1016/J.APCATA.2007.03.021).
- Kamel A.H., Abdallah A.M., El-Baradie H.Y., 1972. The effect of temperature on the properties of calcined red iron oxide pigments. *J. Appl. Chem. Biotech.*, 22, 1209–1215. DOI: [10.1002/JCTB.5020221202](https://doi.org/10.1002/JCTB.5020221202).
- Khanam J., Hasan M.R., Biswas B., Jahan S.A., Sharmin N., Ahmed S., Al-Reza S.M., 2023. Development of ceramic grade red iron oxide pigment from waste iron source. *Heliyon*, 9, e122854. DOI: [10.1016/J.HELİYON.2023.E12854](https://doi.org/10.1016/J.HELİYON.2023.E12854).
- Krześlak A., Hoffmann J., Zieliński S., Maciejewski M., Małek T., 2005. *Najlepsze Dostępne Techniki (BAT) wytyczne dla branży chemicznej w Polsce. Specjalne chemikalia nieorganiczne*. Ministerstwo Środowiska, Warszawa.
- Lu Y., Xu J., Wang W., Wang T., Zong L., Wang A., 2020. Synthesis of iron red hybrid pigments from oil shale semi-coke waste. *Adv. Powder Technol.*, 31, 2276–2284. DOI: [10.1016/J.APT.2020.03.020](https://doi.org/10.1016/J.APT.2020.03.020).
- Mariani F.Q., Borth K.W., Müller M., Dalpasquale M., Anaisi F.J., 2017. Sustainable innovative method to synthesize different shades of iron oxide pigments. *Dyes Pigm.*, 137, 403–409. DOI: [10.1016/j.dyepig.2016.10.024](https://doi.org/10.1016/j.dyepig.2016.10.024).
- Mielicki J., 1997. *Zarys wiadomości o barwie*. Fundacja Rozwoju Polskiej Kolorystyki.
- Namboodiri V.V., Verma R.S., 2001. Microwave-accelerated Suzuki cross-coupling reaction in polyethylene glycol (PEG). *Green Chem.*, 3 146–148. DOI: [10.1039/B102337N](https://doi.org/10.1039/B102337N).
- Pagès G., Leroy S., Sanchez C., 2020. Non-metallurgical iron ore trade in the Roman Mediterranean: an initial synthesis of provenance and use in the case of imperial *Colonia Narbo Martius* (Narbonne, Aude, France). *Archaeol. Anthropol. Sci.*, 12, 140. DOI: [10.1007/S12520-020-01083-5](https://doi.org/10.1007/S12520-020-01083-5).
- Pérez-Arantegui J., 2021. Not only wall paintings—pigments for cosmetics. *Archaeol. Anthropol. Sci.*, 13, 189. DOI: [10.1007/S12520-021-01399-W](https://doi.org/10.1007/S12520-021-01399-W).
- Pfaff G., 2021. Iron oxide pigments. *Phys. Sci. Rev.*, 6, 535–548. DOI: [10.1515/PSR-2020-0179](https://doi.org/10.1515/PSR-2020-0179).
- Pfaff G., 2022. The world of inorganic pigments. *ChemTexts*, 8, 15. DOI: [10.1007/S40828-022-00166-1](https://doi.org/10.1007/S40828-022-00166-1).
- PN-EN ISO 787-5:1999. *Ogólne metody badań pigmentów i wypełniaczy. Oznaczenie liczby olejowej*.
- Rouquerol J., Avnir D., Fairbridge C.W., Everett D.H., Haynes J.M., Pernicone N., Ramsay J.D.F., Sing K.S.W., Unger K.K., 1994. Recommendations for the characterization of porous solids (Technical Report). *Pure Appl. Chem.*, 66, 1739–1758. DOI: [10.1351/PAC199466081739](https://doi.org/10.1351/PAC199466081739).
- Salgado Lopes M.M., de Cássia Silva Sant'Ana Alvarenga R., Gonçalves Pedroti L., Lopes Ribeiro J.C., Fiorini de Carvalho A., de Paula Cardoso F., Cardoso Mendes B., 2019. Influence of the incorporation of granite waste on the hiding power and abrasion resistance of soil pigment-based paints. *Constr. Build. Mater.*, 205, 463–474. DOI: [10.1016/J.CONBUILDMAT.2019.02.046](https://doi.org/10.1016/J.CONBUILDMAT.2019.02.046).
- Sander H., 2020. Colored inorganic pigments, In: McKay R.B. (Ed.), *Technological applications of dispersions*, 105–142. DOI: [10.1201/9781003067252-3](https://doi.org/10.1201/9781003067252-3).
- Sarkodie B., Acheampong C., Asinyo B., Zhang X., Tawiah B., 2019. Characteristics of pigments, modification, and their functionalities. *Color Res. Appl.*, 44, 396–410. DOI: [10.1002/COL.22359](https://doi.org/10.1002/COL.22359).
- Sing K.S.W., Everett D.H., Haul R.A.W., Moscou L., Pierotti R.A., Rouquerol J., Siemieniowska T., 1985. Reporting physisorption data for gas/solid systems with special reference to the determination of surface area and porosity (Recommendations 1984). *Pure Appl. Chem.*, 57, 603–619. DOI: [10.1351/PAC198557040603](https://doi.org/10.1351/PAC198557040603).
- Siqueira-Silva A.I., Rios C.O., Pereira E.G., 2019. Iron toxicity resistance strategies in tropical grasses: The role of apoplastic radicular barriers. *J. Environ. Sci.*, 78, 257–266. DOI: [10.1016/J.JES.2018.10.005](https://doi.org/10.1016/J.JES.2018.10.005).

- Splinter K., 2021. *Otrzymywanie pigmentów żelazowych na bazie odpadowego siarczanu(VI) żelaza(II)*. West Pomeranian University of Technology in Szczecin.
- Splinter K., 2022. *Synteza i charakterystyka tlenków żelaza o właściwościach pigmentacyjnych*. West Pomeranian University of Technology in Szczecin.
- Splinter K., Lenzion-Bieluń Z., 2021. Otrzymywanie pigmentów żelazowych na bazie odpadowego siarczanu(VI) żelaza(II). In: Lenzion-Bieluń Z., Moszyński D. (Eds.), *Postępy w technologii i inżynierii chemicznej 2021*. 240–249. University Publishing House, West Pomeranian University of Technology in Szczecin.
- Splinter K., Lenzion-Bieluń Z., Wojciechowska A., 2021. *Method of producing iron pigments*. Patent No. PL437851A1.
- Splinter K., Moszyński D., Lenzion-Bieluń Z., 2023. Microwave-reactor-based preparation of red iron oxide pigment from waste iron sulfate. *Materials*, 16, 3242. DOI: [10.3390/MA16083242](https://doi.org/10.3390/MA16083242).
- Sreeram K.J., Indumathy R., Rajaram A., Nair B.U., Ramasami T., 2006. Template synthesis of highly crystalline and monodisperse iron oxide pigments of nanosize. *Mater. Res. Bull.*, 41, 1875–1881. DOI: [10.1016/J.MATERRESBULL.2006.03.017](https://doi.org/10.1016/J.MATERRESBULL.2006.03.017).
- Stockman H.M.G., Gevers T., 2000. Color measurement by imaging spectrometry. *Comput. Vision Image Understanding*, 79, 236–249. DOI: [10.1006/cviu.2000.0860](https://doi.org/10.1006/cviu.2000.0860).
- Su C., Wang H., Liu X., 2011. Controllable fabrication and growth mechanism of hematite cubes. *Cryst. Res. Technol.*, 46, 209–214. DOI: [10.1002/CRAT.201000642](https://doi.org/10.1002/CRAT.201000642).
- Tadic M., Trpkov D., Kopanja L., Vojnovic S., Panjan M., 2019. Hydrothermal synthesis of hematite ( $\alpha$ -Fe<sub>2</sub>O<sub>3</sub>) nanoparticle forms: Synthesis conditions, structure, particle shape analysis, cytotoxicity and magnetic properties. *J. Alloys Compd.*, 792, 599–609. DOI: [10.1016/J.JALLCOM.2019.03.414](https://doi.org/10.1016/J.JALLCOM.2019.03.414).
- Touazi Y., Abdi A., Leshaf A., Khimeche K., 2020. Influence of heat treatment of iron oxide on its effectiveness as anticorrosion pigment in epoxy based coatings. *Prog. Org. Coat.*, 139, 105458. DOI: [10.1016/J.PORGCOAT.2019.105458](https://doi.org/10.1016/J.PORGCOAT.2019.105458).
- Wang Y., Xue S., Lin Q., Song D., He Y., Liu L., Zhou J., Zong M., De Yoreo J.J., Zhu J., Rosso K.M., Sushko M.L., Zhang X., 2022. Particle-based hematite crystallization is invariant to initial particle morphology. *PNAS*, 119, e2112679119. DOI: [10.1073/PNAS.2112679119](https://doi.org/10.1073/PNAS.2112679119).
- Wolska E., 1988. Relations between the existence of hydroxyl ions in the anionic sublattice of hematite and its infrared and X-ray characteristics. *Solid State Ionics*, 28–30, Part 2, 1349–1351. DOI: [10.1016/0167-2738\(88\)90385-2](https://doi.org/10.1016/0167-2738(88)90385-2).
- Wolska E., Schwertmann U., 1989. Nonstoichiometric structures during dehydroxylation of goethite. *Zeitschrift Für Kristallographie – Crystalline Materials*, 189, 223–238. DOI: [10.1524/ZKRI.1989.189.14.223](https://doi.org/10.1524/ZKRI.1989.189.14.223).